The effects of paroxetine-induced transient apoptosis and brain remodeling on social behavior in developing zebrafish

Tomomi Sato,[1,2]* Kaito Saito,[3] Tsubasa Oyu,[3] Sachiko Tsuda,[3] Tomohiro Kurisaki,[1] Takeshi Kajihara,[2] Masabumi Nagashima[1]

[1]Department of Anatomy, School of Medicine, Saitama Medical University, Morohongo 38, Moroyama-machi, Saitama 350-0495, Japan
[2]Department of Obstetrics and Gynecology, School of Medicine, Saitama Medical University, Morohongo 38, Moroyama-machi, Saitama 350-0495, Japan
[3]Division of Life Science, Graduate School of Science and Engineering, Saitama University, 255 Shimo-Okubo, Sakura-ku, Saitama City, Saitama 338-8570, Japan

*Corresponding author
[1]Department of Anatomy, School of Medicine, Saitama Medical University, Morohongo 38, Moroyama-machi, Saitama 350-0495, Japan
Tel: +81-49-276-1148
Fax: +81-49-276-1148
Email: tosato@saitama-med.ac.jp (TS)

Abstract

Autism spectrum disorder (ASD) is a neurodevelopmental condition caused by various genetic and environmental factors. This disorder has the cardinal symptoms including impaired social behavior involving the amygdala. Antidepressants such as paroxetine in early pregnancy increase the risk of ASD in offspring. However, a comprehensive picture of the underlying pathogenic mechanisms remains elusive. Here, we demonstrate that early exposure of zebrafish embryos to paroxetine suppresses neurogenesis in the optic tectum and the dorsal telencephalon which corresponds to the human amygdala. Paroxetine-treated embryos exhibit impaired growth, with small heads and short body lengths resulting from transient apoptosis. This is reminiscent of the early-onset fetal growth restriction (FGR) associated with ASD. Interestingly, the suppressed neurogenesis in the small heads was found to be restored after the cessation of paroxetine. This was accompanied by extended retinotectal projections, suggesting brain-preferential remodeling. Finally, the paroxetine-treated fish exhibited impaired social behavior, further supporting the correspondence with ASD. Our findings offer new insights into the early neurodevelopmental etiology of ASD.

Introduction

Autism spectrum disorder (ASD) is a neurodevelopmental disorder diagnosed in childhood[1]. The cardinal symptoms include impaired social behavior, communication disorder, and stereotyped repetitive behaviors[2]. To date, a large number of genes have been identified as related to ASD. These are involved in synaptic functions, transcriptional regulation, and brain development[1,3]. Furthermore, *de novo* mutations, paternal age, maternal infection and inflammation during pregnancy have also been implicated as causative factors[3–5]. Thus, various genetic and environmental factors contribute to the impaired brain development and functions observed in ASD[4–6]. Maternal depression and anxiety during pregnancy are also associated with an increased risk of ASD in offspring[7]. Selective-serotonin reuptake inhibitors (SSRIs), one of the conventional types of antidepressants, are prescribed to pregnant women based on risk-benefit considerations[8]. The drugs act on the maternal brain to exert their therapeutic effects but also pass through the placenta to the fetus[9,10]. Several studies suggest that maternal use of SSRIs during the first trimester of pregnancy increases the risk of ASD[11–14]. However, a comprehensive picture of the underlying pathogenic mechanisms remains elusive.

Fetal growth restriction (FGR) is a common complication during pregnancy and possibly caused by various maternal, placental, and fetal factors[15]. Early-onset (type I) FGR manifests as a morphologically symmetrical fetus with a small head and body due to fetal growth failure[16]. The causative factors include genetic abnormalities, congenital malformation, intrauterine infection, and the teratogenic effect[15]. This type of FGR is also associated with ASD[17–19]. However, the pathophysiological role of SSRIs in type 1 FGR is poorly understood.

Serotonin (5-hydroxytryptamine [5-HT]) is a monoamine neurotransmitter involved in emotional disorders such as depression and anxiety by modulating synaptic transmission in the brain[20,21]. SSRIs exert their therapeutic effects by inhibiting the reuptake of 5-HT via SERT 5-HT transporters, to sustain concentrations of extracellular 5-HT[22,23]. 5-HT also plays an important role in adult neurogenesis by promoting the self-renewal of neural stem cells in the hippocampus[24]. Moreover, maternal 5-HT synthesized in the placenta of pregnant mice has been found to transiently localize in the forebrain of early-stage embryos[25], raising the possibility that placenta-derived 5-HT regulates early brain development[26–28]. ⁻However, the effects of early-stage SSRI and 5-HT on embryonic brain development and postnatal behaviors are unclear.

Here, we address the effects of SSRI exposure during early embryogenesis on brain

development and subsequent social behavior. For early prediction and prevention of the risk for ASD, elucidation of the primary causes is essential. The involvement of various genetic and environmental factors makes it difficult to comprehensively understand the causes and consequences for the pathogenetic mechanisms of ASD[1–4]. While SSRI during early pregnancy increases the risk of ASD, the primary cause remains unclear[11,13,14]. Thus, there is a need to elucidate the primary actions of SSRI exposure on early brain development and the subsequent effects on social behavior, which is the aim of this study. For this purpose, we use a zebrafish model because of easy access to early embryos in a living and intact condition for the investigation of direct actions on those embryos. In addition, various model systems for neurodevelopmental disorders have already been established in zebrafish and there appears to be evolutionary conservation of the pathophysiological mechanisms underlying the disorders between humans and zebrafish[29–31]. We focus on the SSRI, paroxetine, because of its broad applicability across affective disorders, including major depressive and anxiety disorders[32]. Moreover, the three-dimensional structures of paroxetine-binding sites and interacting amino acids in human SERT have been well-defined by X-ray crystallography[33,34]. In this study, we assess the effects of paroxetine and compare those with the control and 5-HT, on morphology, neurogenesis, projection in the brain during embryonic, larval stages, and finally on social behavior in juvenile stages.

Results

Paroxetine suppresses neurogenesis to increase the number of neural progenitor cells in the optic tectum

To investigate the effects of paroxetine on brain development in zebrafish embryos, we first examined to what extent SERT, a 5-HT transporter targeted by paroxetine, is conserved between humans and zebrafish. We found that the entire amino acid sequence is 70% identical between the two species. All the amino acids that interact with paroxetine in human SERT binding sites were identical between the two species (Supplementary Fig. S1)[33]. SERT proteins were found to be broadly expressed in the brains of embryonic zebrafish at 24 hours post-fertilization (hpf). This is prior to the development of serotonergic neurons in the raphe nuclei (Supplementary Fig. S2)[35]. SERT proteins were localized to the apical surfaces of radial glial cells in the ventricular zone (Supplementary Fig. S2), suggesting that SERT is involved in neural stem/progenitor cells.

We treated zebrafish embryos with 10 μM paroxetine between 26–50 hours-post fertilization (hpf), which roughly corresponds to the first trimester of human pregnancy, and examined the effect of the drug on neurogenesis in the brain. This was done using the transgenic lines TgBAC(*neurod1:EGFP*), expressing enhanced green fluorescent protein (EGFP) in differentiated neurons[36], and Tg(*elavl3:kaede*), expressing Kaede under a pan-neuronal promoter[37] (Fig. 1a, Supplementary Fig. S3). Fluorescence intensity was quantified, because it is proportional to the number of post-mitotic neurons and the time since differentiation[31]. We found this to be significantly decreased in the optic tectum and the telencephalon of the paroxetine-treated embryos compared to the control dimethylsulfoxide (DMSO)-treated embryos, indicating that the paroxetine had suppressed neurogenesis (Fig. 1b, c, Supplementary Fig. S3). To examine whether the effect of paroxetine on neurogenesis is mediated by the upregulation of extracellular 5-HT, we treated embryos at the same developmental stage with 5-HT. Consistent with paroxetine-treated embryos, the EGFP intensity was significantly decreased in the optic tectum of the 5-HT-treated embryos compared to the controls, indicating that the effect of paroxetine is reproducible with 5-HT (Fig. 1b, c).

In adult neurogenesis of both rodents and humans, SSRIs are known to promote the proliferation of neural stem cells[24,50]. Therefore, we examined the proliferation of neural stem/progenitor cells in the optic tectum using anti-phospho-histone H3 (pH3) antibody[31]. We found that paroxetine-treated embryos showed an increase in the number of pH3-positive mitotic cells in the optic tecta at 50 hpf (Fig. 1d, e). This was selectively detected in the subventricular zone (SVZ) (Fig. 1d, f, g). In the developing brain, neurons are

generated from neural stem/progenitor cells at the expense of the proliferation of those cells[31,66]. Thus, we examined the expression of SOX2, a marker of neural stem/progenitor cell proliferation[38]. SOX2 was significantly increased in paroxetine-treated embryonic brains, with a concomitant decrease in Kaede expression at 48 and 50 hpf (Fig. 1h, i, Supplementary Fig. S3). These results suggest that paroxetine promotes the proliferation of neural stem/progenitor cells by suppressing neurogenesis in the optic tectum.

Next, we explored whether apoptosis was induced in the paroxetine-treated brain by immunostaining with antibodies against active Caspase-3 at 48 hpf. The intensity of the Caspase-3-positive signals was significantly decreased in the optic tecta and the telencephalons of paroxetine-treated embryos, indicating the suppression of apoptosis in the paroxetine-treated brains (Fig. 1j–l). We then examined the expression of Ras homolog gene family member A (RhoA) because the GTP-binding protein suppresses apoptosis in zebrafish embryos and also exhibits increased expression in the brain of ASD model, *Kctd13*-deficient mice[39–41]. RhoA proteins were significantly increased in the optic tecta of paroxetine-treated embryos compared to the controls (Fig. 1m, n).

Paroxetine induces local apoptosis, generating embryos with short body lengths and small heads

To clarify the effects of paroxetine exposure on embryonic development, we measured the head-tail body length and head area of paroxetine-treated zebrafish embryos to parallel the indication of human fetal development estimated by crown-lump length (CRL) between weeks 8–11 of the first trimester in human pregnancy. We first monitored the typical development of wild-type embryos. In these, body lengths and head areas were gradually but significantly greater than those embryos at 50 hpf, according to developmental stages (Supplementary Fig. S4). Embryos treated with 10 μM paroxetine exhibited restricted growth with a slight but significant decrease in body length and head area at 50 hpf (Fig. 2a–c). This closely resembled early-onset FGR in the first trimester of human embryonic development[16]. In contrast to the similar effects of paroxetine and 5-HT on neurogenesis observed in the optic tectum (Fig. 1b, c), 5-HT did not affect the body length or head area of the embryos (Fig. 2a–c). This indicated that the observed embryonic growth restriction was a paroxetine-selective action. To elucidate the mechanisms underlying the different effects of paroxetine and 5-HT on embryonic morphology, we examined the induction of apoptosis at 31 hpf, 5 hours after treatment with paroxetine or 5-HT (Fig. 2d). We found a significant increase in the immunofluorescent signal intensity of active Caspase-3 in paroxetine-treated embryos compared to the DMSO control embryos. However, no such increase was detected in 5-

168 HT-treated embryos (Fig. 2e, g). Similarly, growth restriction and increased apoptosis
169 were observed in *slc6a4a* (*serta*)-knockdown embryos (Supplementary Fig. S2). These
170 results indicate that the increased apoptosis observed was caused by reduced 5-HT
171 transportation due to the inhibition of SERT. The apoptosis was induced by paroxetine in
172 a dose-dependent manner (Fig. 2h). Co-treatment with paroxetine and 5-HT also
173 increased apoptosis (Fig. 2i). These suggest that the apoptosis is not mediated by
174 increased extracellular 5-HT activating 5-HT receptors, but instead predominantly caused
175 by paroxetine blocking the incorporation of 5-HT via SERT. Moreover, in addition to the
176 apoptosis observed in the brain, it was also locally and specifically induced in the tail tip
177 of paroxetine-treated embryos in an all-or-nothing manner (Fig. 2f, j). These results
178 indicate that the local apoptosis induced by paroxetine in the brain and tail tip of zebrafish
179 embryos is responsible for the decreased head area and body length.
180

181 **Early transient paroxetine impairs the development of retinotectal projections**
182 **which are later restored with extended retinal axons**

183 To investigate whether the suppressed neurogenesis in paroxetine-treated embryos
184 affected later neural circuit formation, we examined the retinotectal projections in the
185 optic tecta. We used transgenic line Tg(*pou4l-hsp70l:GFP*) expressing GFP in excitatory
186 tectal neurons and retinal ganglion cells (RGCs), and line
187 Tg(*pou4f3:GAL4;UAS:mCherry*) expressing mCherry in RGCs[42–43]. For wild-type larvae,
188 GFP- and mCherry-expressing areas were gradually but significantly larger in the optic
189 tecta than those larvae at 72 hpf, according to developmental progression (Supplementary
190 Fig. S4). In contrast, the fluorescence intensity of both the GFP-expressing and mCherry-
191 expressing areas was significantly decreased between 5 and 7 days post fertilization (dpf;
192 Supplementary Fig. S4). As activity-dependent competition and dynamic synapse
193 formation occur in retinal axons and tectal dendrites, respectively, during these
194 developmental stages, it could be inferred from our result that this parameter can detect
195 refinement of the projection[44,45]. Treatment with 1 μM paroxetine for two days caused
196 significant decreases in both the area and the fluorescence intensity of the optic tectum
197 regions expressing GFP and mCherry at 73 hpf (Fig. 3a–e, Supplementary Fig. S5). As
198 previously mentioned, these paroxetine-treated larvae exhibited significantly shorter
199 body lengths and smaller head areas (Supplementary Fig. S5). Treatment with 10 μM
200 paroxetine for one day had a similar effect on larval morphology and retinotectal
201 projection development at 3 dpf (Supplementary Fig. S5), indicating that transient early-
202 stage treatment is sufficient for paroxetine to exert its growth-inhibiting effects.
203 We next investigated the effects of early transient paroxetine on later development in

the retinotectal projection. Similar to 3-dpf larvae, 5-dpf larvae treated with paroxetine during 26–50 hpf showed significant decreases in body lengths, head areas, and in the area and the intensity of the GFP-expressing region in the optic tecta compared to the controls (Supplementary Fig. S6). Interestingly, we found that the paroxetine-treated larvae exhibited restoration of their head areas compared to the controls at 7 dpf but persistent significant decreases in their body lengths (Fig. 3f–i), suggesting that brain-preferential remodeling occurred between 5–7 dpf. Consistent with the head area restoration, paroxetine-treated 7-dpf larvae exhibited restoration of both the areas and the intensities of the GFP-expressing regions and the intensities of the mCherry-expressing regions in their optic tecta. These all reverted to values equivalent to those in the controls (Fig. 3j–l, n). Furthermore, the areas of mCherry-expressing regions were significantly expanded in paroxetine-treated larvae compared to the controls (Fig. 3m). This expansion was recapitulated in 5-HT-treated larvae (Fig. 3m), suggesting that early transient paroxetine treatment drives the extension of retinal axons through 5-HT at later neurodevelopmental stages.

Early paroxetine administration negatively affects neurogenesis in the dorsal telencephalon, contributing to a tendency toward impaired social behavior

The amygdala plays a critical role in social behavior but is dysfunctional in ASD, causing the impaired social behavior characteristic of ASD[2]. In individuals with ASD, research has found that the number of neurons in the amygdala do not undergo neurotypical alterations during their development[46]. Therefore, we investigated whether early paroxetine administration in zebrafish affects the development of the dorsal telencephalon, which corresponds to the mammalian amygdala[29]. The SAGFF120A gene-trap line expressing Gal4FF in dorsal telencephalon neurons essential to active avoidance fear conditioning, was used to assess the effects of paroxetine[47]. As in the optic tecta, the fluorescence intensity of the GFP-expressing areas was significantly decreased in the dorsal telencephalons of paroxetine- and 5-HT-treated embryos compared to the control at 48 hpf (5-HT, $p = 0.00161$, Fig. 4a, b), and 76 hpf (parox, $p = 0.0279$; 5-HT, $p = 0.0250$, Supplementary Fig. S7). However, the GFP intensity in the dorsal telencephalon was restored at 7 dpf following washout of paroxetine and 5-HT at 2 dpf (Parox, $p = 0.1419$; 5-HT, $p = 0.6623$; Fig. 4c–f). Again, this restoration was consistent with the results observed in the embryonic optic tecta (Fig. 3, Supplementary Fig. S7).

Finally, we explored whether these effects of early transient paroxetine treatment affected juvenile social behavior. To assess social behavior in young fish, we developed a behavioral apparatus using a test case separated into three chambers: a test area, a sibling

area, and a non-sibling area (Fig. 5a; see Methods). The swimming trajectories of the fish in the absence (non-sibling trial) or presence (sibling trial) of siblings were recorded and analyzed for the location of the fish in the sibling frame (blue) or non-sibling frame (red) to examine whether there was a social preference for the sibling frame. This was measured by calculating the social preference index (SPI, $-1 < SPI < 1$) (Fig. 5b, c; Supplementary Videos 1–6; see Methods). Our behavioral analysis revealed that the incidence of positive SPI (sibling trial > non-sibling trial) was lower in the fish treated with paroxetine or 5-HT than in the control fish. In contrast, the incidence of negative SPI (sibling trial < non-sibling trial) was increased in the paroxetine- and 5-HT-treated fish compared to the control fish (Fig. 5d; DMSO, n = 13; parox, n = 7; 5-HT, n = 6). The SPI differences between the sibling and non-sibling trials were not significant but more negative in paroxetine and 5-HT than the control, suggesting a tendency to impaired social behavior ($p = 0.0456$, Brown-Forsythe ANOVA test; Fig. 5e). Total distances of swimming trajectories were always lower in the sibling trials, producing negative values for differences between the sibling and non-sibling trials in the control (Fig. 5f). The decreased total distances in the sibling trials were also observed in paroxetine-treated fish (Fig. 5f), whereas a significant increase in the differences was detected in the 5-HT-treated fish compared to the control and paroxetine fish (control, $p = 0.0427$; parox, $p = 0.0082$; Fig. 5f). These results indicate a difference in the behavioral effects of early transient exposure to paroxetine and 5-HT.

Discussion

In this study, we reveal that paroxetine- and 5-HT-treated zebrafish embryos exhibit suppressed neurogenesis in the optic tectum, with increased expression of SOX2, a marker of proliferating neural stem/progenitor cells in the brain[48]. Despite this suppressed neurogenesis, the number of pH3-positive mitotic cells are selectively increased in the subventricular zone, indicating that the proliferation of neural stem/progenitor cells is promoted by paroxetine at the expense of neurogenesis in the brain. Our results suggest that paroxetine expands the number of neural stem/progenitor cells in the zebrafish embryonic brain. This is consistent with the effect of SSRI that increases the number of neural stem/progenitor cells in the dentate gyrus of the adult mammalian hippocampus through the increased concentration of 5-HT[24,49,50]. These results also suggest that, while SSRI use during pregnancy can have therapeutic effects on the human maternal brain, it is likely to have adverse effects on the embryonic brain. We show that apoptosis is suppressed in the paroxetine-treated brain of zebrafish embryos. Similar effects have previously been observed in SERT-knockout mice, which exhibit reductions in programmed cell death in the brain[51]. The increased expression of RhoA proteins in the paroxetine-treated optic tectum is supported by the observation that RhoA prevents apoptosis during embryonic development in zebrafish[39]. These findings raise the possibility that anti-apoptotic signaling through RhoA is a common pathway shared among ASD models, including *Kctd13*-deficient mice, in which increased RhoA reduces synaptic transmission[40,41].

Next, we show that early embryonic exposure to paroxetine restricts growth, resulting in short body lengths and small heads in zebrafish. In humans, early-onset FGR manifests as symmetrical morphology with a small head and body, in which the causative factors include the teratogenic effect[15,16]. Thus, the paroxetine-treated zebrafish embryos are considered as a model of early-onset (type I) FGR in humans. The growth restriction is induced by paroxetine but not by 5-HT which is incorporated into cells through SERT, the target protein blocked by paroxetine. Similarly, apoptosis is locally induced by paroxetine in the brain and the tail tip, but not by 5-HT, indicating disparities between the effects of paroxetine and 5-HT on embryogenesis. Our results suggest that apoptosis is the underlying mechanism for the paroxetine-induced embryonic growth restriction. Indeed, SSRIs such as paroxetine have already been reported to induce apoptosis in various malignant cell types, including gliomas, neuroblastomas, leukemia, lymphomas, and colon tumors, in addition to normal cells such as myeloid cells, osteoblasts, and osteoclasts[52–55]. These lines of evidence suggest a shared mechanism of action of SSRIs

298 for the apoptosis induction in proliferating cells, potentially attributable to the etiology of
299 adverse effects of SSRIs on embryogenesis. In contrast, another SSRI, fluvoxamine, has
300 recently been identified that have therapeutic potential as an immunomodulator due to its
301 ability to suppress immune responses. This is likely to reduce the risk of deterioration in
302 COVID-19[56,57]. These pleiotropic effects of SSRIs are reminiscent of those of
303 thalidomide. This is because thalidomide also has proapoptotic properties to exert
304 teratogenic effects on embryogenesis, and the exposure during early pregnancy has been
305 associated with later ASD[67,68]. The drug can similarly be used therapeutically for
306 immunomodulation[58,59].
307 We prove that suppressed neurogenesis in early paroxetine-treated embryos decreases
308 the areas and intensity of the retinotectal projection, which is restored at a later
309 neurodevelopmental stage after the removal of all paroxetine from the brain. Likewise,
310 head size is restored at a later stage in such embryos; however, body length is not,
311 indicating brain-preferential remodeling. These raise the possibility that remodeling also
312 occurs in neural networks of those embryonic brains during the restoration stages,
313 because those stages correspond to the period of activity-dependent refinement in the
314 retinotectal projection[44,45]. Indeed, we show extended retinal axon projections in the
315 restored brain. This axonal projection phenotype is similar to that observed in SERT-
316 knockout mice exhibiting impaired segregation of retinal axons both in the superior
317 colliculus and the dorsal lateral geniculate nucleus, leading to the disruption of sensory
318 map formation[60,61]. The extended axons are also observed in embryos treated with 5-HT,
319 suggesting that this paroxetine effect is mediated by 5-HT. Our observations suggest that
320 growth restriction and suppressed neurogenesis affect later neural circuit formation and
321 refinement during brain development, providing a neurobiological basis for the
322 pathogenesis of ASD as well as other neurodevelopmental disorders associated with FGR.
323 Early paroxetine- and 5-HT-induced suppression of neurogenesis followed by its
324 restoration is also observed in the dorsal telencephalon corresponding to the mammalian
325 amygdala, which has been shown to play a critical role in active avoidance fear
326 conditioning using the gene-trap line, SAGFF120A[29,47]. Our results suggest that
327 remodeling of neural circuits occurs in both the optic tectum and the dorsal telencephalon
328 of both paroxetine- and 5-HT-treated larvae since the suppressed neurogenesis was
329 completed at a later stage in both larvae. Furthermore, we explore the implications of
330 suppressed neurogenesis for the development of social behavior. The SPI differences in
331 the control are broadly distributed overlapping with those more negatively distributed in
332 paroxetine- and 5-HT-treated fish, and thereby these are not significantly different in
333 comparison with the control. However, the incidence of negative SPI is markedly

increased in both treated fish. Therefore, our behavioral analyses demonstrate the negative impact of early exposure to paroxetine and 5-HT on the development of social behavior with a broad spectrum of their impacts. This implies that the impaired social behavior we observed may be attributable to suppressed neurogenesis and subsequent brain remodeling induced by other genetic and environmental factors. Interestingly, the difference in total swimming distances is significantly different between fish treated with paroxetine and 5-HT, implying a difference in the effects of the two compounds on neural circuits involved in social behavior. These findings offer new insights into the neurodevelopmental mechanisms underlying the etiology of ASD. However, a more detailed analysis of the structure and function of the relevant neural circuits is necessary to fully understand the brain remodeling mechanisms and the differing effects of brain exposure to paroxetine and 5-HT. Nevertheless, our study provides evidence for the effects of paroxetine and 5-HT on embryonic brain development and the consequent effects on social behavior. Furthermore, it also provides a simple screening system for the evaluation of contributing factors affecting social behavior in zebrafish.

351 # Methods

352

353 **Zebrafish maintenance and strains.**

354 Wild-type and transgenic zebrafish were kept at 28ºC under 14 hours:10 hours light/dark
355 cycles as described previously (Westerfield, 5th Ed. 2007). To obtain transgenic embryos,
356 a wild-type strain Riken WT (RW) was crossed with transgenic lines as follows:
357 Tg(*elavl3:Kaede*) to visualize post-mitotic neurons[1]; TgBAC(*neurod1:EGFP*) to
358 visualize differentiated neurons; Tg(*pau4f1-hsp70l:gfp*) to visualize development of post-
359 mitotic excitatory neurons and retinal axons in the optic tectum[2];
360 Tg(*pau4f3:GAL4;UAS:mCherry*) to visualize retinal axons in the optic tectum[3]; and
361 SAGFF120A;UAS:GFP to visualize neurons in the dorsal telencephalon[4]. All animal
362 experiments for this study were approved by the Animal Experimentation Committee of
363 Saitama Medical University and performed in accordance with the Regulation on Animal
364 Experimentation at Saitama Medical University. This study was carried out in compliance
365 with the ARRIVE guidelines.

366

367 **Microinjection.**

368 Antisense morpholino oligonucleotides (MO) were diluted in 1× Danieau buffer (58 mM
369 NaCl, 0.7 mM KCl, 0.4 mM $MgSO_4$, 0.6 mM $Ca(NO_3)_2$, 5.0 mM HEPES, pH 7.6) and
370 injected into 1 to 2-cell-stage embryos by using a microinjector FemtoJet 5247
371 (Eppendorf). The sequences and the concentrations of MOs (Gene Tools) used in this
372 study are as follows: slc6a4a-AMO (AMO; splice-blocking, MO1-slc6a4a, ZDB-
373 MRPHLNO-141031-1, ZIRC), 5'- ACGCACTTACATGCACTTACACATA -3', at 4.178
374 ng/nl; slc6a4a-5mis (5mis; 5-bp-mismatched control), 5'-
375 ACCCACTTAGATCCAGTTAGACATA -3', at 4.198 ng/nl.

376

377 **Drug treatments.**

378 Preparation of paroxetine and 5-HT solution were carried out as previously described [5].
379 Briefly, paroxetine or 5-HT were dissolved in DMSO at 10 mM for stock solutions and
380 diluted with E3 medium (5 mM NaCl, 0.17 mM KCl, 0.33 mM $MgSO_4$, 0.33 mM $CaCl_2$)
381 to adjust the final concentration to 1 or 10 μM in 1% DMSO. Zebrafish embryos were
382 dechorionated with forceps and immersed in the solution from 26-27 hpf, and then
383 incubated at 28.5ºC.

384

385 **Immunohistochemistry.**

386 Whole-mount immunohistochemistry was carried out by overnight incubation of 4%

387 paraformaldehyde/PBS-fixed embryos with primary antibodies at 4ºC, followed by
388 incubation with secondary antibodies against rabbit or goat IgG conjugated with Alexa
389 Flour 488 or 555 (Abcam) together with DAPI (Thermo Fisher Scientific). The following
390 primary antibodies were used in this study: anti-active Caspase-3 (rabbit, 1:500 dilution,
391 BD Pharmingen 559565); anti-phospho histone H3 (pH3; 1:500 dilution, Cell Signaling
392 9701); Sox2 (rabbit, 1:500 dilution, GeneTex GTX124477); anti-Serotonin (goat, 1:500
393 dilution, Abcam ab66047); SLC6S4/5-HTT (rabbit, 1:100 dilution, Thermo Fisher
394 Scientific PA5-49572). Following immunostaining, phosphate-buffered saline (PBS), the
395 wash solution of embryos was gradually substituted by 30%, 50% and finally 70%
396 glycerol/PBS for imaging under a microscope.
397
398 **Microscopy and imaging.**
399 Images were captured using a stereoscopic microscope Leica MZ10F equipped with
400 MC170 HD camera, and a confocal laser scanning microscope Zeiss LSM700 equipped
401 with EC Plan-NEOFLUAR 20×/NA 0.5 and LD Plan-NEOFLUAR 40×/NA 0.6
402 objectives. Each confocal image was obtained by compiling approximately 30–40 optical
403 sections at 2.0 µm intervals using a sequential-scanning mode for multicolor fluorescence
404 imaging.
405
406 **Social behavioral analysis.**
407 A test case (68 mm depth × 39 mm width × 15 mm height) divided into three
408 compartments (sibling, no sibling areas, 10-mm depth on both sides; test area, 48-mm
409 depth in the center) was used to observe social behaviors of young fish (35–37 dpf).
410 Swimming behaviors in the test case were recorded by capturing movies using a Blackfly
411 camera (fps 100) for 5 min at 50 frames per sec (fps). Each experiment was performed in
412 order of five steps as follows: (1) A fish was transferred to the test area and habituated for
413 5 min. (2) Without siblings, swimming behavior was recorded for 5 min (no sibling trial).
414 (3) Siblings were transferred to the sibling area and habituated for 5min. (4) With siblings,
415 swimming behavior was recorded for 5 min (sibling trial). (5) Captured movies were
416 converted to .avi format using ImageJ software, and tracking analysis of the swimming
417 fish was performed using UMATracker software (Release 15). Social behaviors were
418 analyzed by comparing (2) with (4) for Social Preference Index (SPI) calculated as
419 follows: SPI = (Sibling frames – No sibling frames) / Total frames. Sibling frames (blue)
420 were defined as fish located in a half region on the side of sibling area, while no sibling
421 frames (red) were defined as fish located in the other region in the test area. A value of
422 SPI varied between –1 and 1[6]. SPI difference is positive when SPI in the sibling trial is

larger than the no sibling trial, and negative when SPI in the sibling trial is smaller than the no sibling trial. Difference in total distance was defined as the value in sibling trial subtracting that in no sibling trial.

Quantification and statistical analysis.

Body length, head area and Kaede, GFP or mCherry-positive areas and intensities were measured using Adobe Photoshop (2023, Ver. 24.4.1). A z-stacked image by confocal laser scanning microscopy is binarized above a threshold larger than 3 pixels, which is defined as the fluorescence-positive area, and the area and the fluorescence mean intensity are measured. For statistical analysis of two or more samples, two-tailed, unpaired nonparametric Mann-Whitney U test or Kruskal-Wallis with Dunn's multiple comparison tests were performed, unless otherwise noted, using GraphPad Prism 9 (Ver. 9.5.1).

Data Availability

All data generated or analyzed during this study are available from the corresponding author on reasonable request.

443 ## References

444

445 1. Sestan N, State MW. Lost in Translation: Traversing the Complex Path from
446 Genomics to Therapeutics in Autism Spectrum Disorder. *Neuron* **100**, 406-423
447 (2018).
448 2. Amaral DG, Schumann CM, Nordahl CW. Neuroanatomy of autism. *Trends*
449 *Neurosci* **31**, 137-145 (2008).
450 3. Iakoucheva LM, Muotri AR, Sebat J. Getting to the Cores of Autism. *Cell* **178**,
451 1287-1298 (2019).
452 4. Willsey HR, Willsey AJ, Wang B, State MW. Genomics, convergent
453 neuroscience and progress in understanding autism spectrum disorder. *Nat Rev*
454 *Neurosci* **23**, 323-341 (2022).
455 5. Al-Haddad BJS*, et al.* The fetal origins of mental illness. *Am J Obstet Gynecol*
456 **221**, 549-562 (2019).
457 6. Amgalan A, Andescavage N, Limperopoulos C. Prenatal origins of
458 neuropsychiatric diseases. *Acta Paediatr* **110**, 1741-1749 (2021).
459 7. Wiggins LD*, et al.* A Phenotype of Childhood Autism Is Associated with
460 Preexisting Maternal Anxiety and Depression. *J Abnorm Child Psychol* **47**, 731-
461 740 (2019).
462 8. Howard LM, Molyneaux E, Dennis CL, Rochat T, Stein A, Milgrom J. Non-
463 psychotic mental disorders in the perinatal period. *Lancet* **384**, 1775-1788
464 (2014).
465 9. Hendrick V, Stowe ZN, Altshuler LL, Hwang S, Lee E, Haynes D. Placental
466 passage of antidepressant medications. *Am J Psychiatry* **160**, 993-996 (2003).
467 10. Ewing G, Tatarchuk Y, Appleby D, Schwartz N, Kim D. Placental transfer of
468 antidepressant medications: implications for postnatal adaptation syndrome. *Clin*
469 *Pharmacokinet* **54**, 359-370 (2015).
470 11. Croen LA, Grether JK, Yoshida CK, Odouli R, Hendrick V. Antidepressant use
471 during pregnancy and childhood autism spectrum disorders. *Arch Gen*
472 *Psychiatry* **68**, 1104-1112 (2011).
473 12. Velasquez JC, Goeden N, Bonnin A. Placental serotonin: implications for the
474 developmental effects of SSRIs and maternal depression. *Front Cell Neurosci* **7**,
475 47 (2013).
476 13. Millard SJ, Weston-Green K, Newell KA. The effects of maternal antidepressant
477 use on offspring behaviour and brain development: Implications for risk of
478 neurodevelopmental disorders. *Neurosci Biobehav Rev* **80**, 743-765 (2017).

14. Andalib S, *et al.* Maternal SSRI exposure increases the risk of autistic offspring: A meta-analysis and systematic review. *Eur Psychiatry* **45**, 161-166 (2017).
15. Nardozza LM, *et al.* Fetal growth restriction: current knowledge. *Arch Gynecol Obstet* **295**, 1061-1077 (2017).
16. Dall'Asta A, Brunelli V, Prefumo F, Frusca T, Lees CC. Early onset fetal growth restriction. *Matern Health Neonatol Perinatol* **3**, 2 (2017).
17. Pels A, *et al.* Neurodevelopmental outcomes at five years after early-onset fetal growth restriction: Analyses in a Dutch subgroup participating in a European management trial. *Eur J Obstet Gynecol Reprod Biol* **234**, 63-70 (2019).
18. Ranzil S, *et al.* Disrupted placental serotonin synthetic pathway and increased placental serotonin: Potential implications in the pathogenesis of human fetal growth restriction. *Placenta* **84**, 74-83 (2019).
19. Joseph RM, *et al.* Extremely low gestational age and very low birthweight for gestational age are risk factors for autism spectrum disorder in a large cohort study of 10-year-old children born at 23-27 weeks' gestation. *Am J Obstet Gynecol* **216**, 304 e301-304 e316 (2017).
20. Gaspar P, Cases O, Maroteaux L. The developmental role of serotonin: news from mouse molecular genetics. *Nat Rev Neurosci* **4**, 1002-1012 (2003).
21. Pourhamzeh M, *et al.* The Roles of Serotonin in Neuropsychiatric Disorders. *Cell Mol Neurobiol* **42**, 1671-1692 (2022).
22. Otte C, *et al.* Major depressive disorder. *Nat Rev Dis Primers* **2**, 16065 (2016).
23. Gross C, *et al.* Serotonin1A receptor acts during development to establish normal anxiety-like behaviour in the adult. *Nature* **416**, 396-400 (2002).
24. Aimone JB, Li Y, Lee SW, Clemenson GD, Deng W, Gage FH. Regulation and function of adult neurogenesis: from genes to cognition. *Physiol Rev* **94**, 991-1026 (2014).
25. Bonnin A, *et al.* A transient placental source of serotonin for the fetal forebrain. *Nature* **472**, 347-350 (2011).
26. Rosenfeld CS. The placenta-brain-axis. *J Neurosci Res* **99**, 271-283 (2021).
27. St-Pierre J, Laurent L, King S, Vaillancourt C. Effects of prenatal maternal stress on serotonin and fetal development. *Placenta* **48 Suppl 1**, S66-S71 (2016).
28. Trowbridge S, Narboux-Neme N, Gaspar P. Genetic models of serotonin (5-HT) depletion: what do they tell us about the developmental role of 5-HT? *Anat Rec (Hoboken)* **294**, 1615-1623 (2011).
29. Rea V, Van Raay TJ. Using Zebrafish to Model Autism Spectrum Disorder: A Comparison of ASD Risk Genes Between Zebrafish and Their Mammalian

515 Counterparts. *Front Mol Neurosci* **13**, 575575 (2020).
516 30. Sakai C, Ijaz S, Hoffman EJ. Zebrafish Models of Neurodevelopmental
517 Disorders: Past, Present, and Future. *Front Mol Neurosci* **11**, 294 (2018).
518 31. Sato T*, et al.* Neuregulin 1 Type II-ErbB Signaling Promotes Cell Divisions
519 Generating Neurons from Neural Progenitor Cells in the Developing Zebrafish
520 Brain. *PLoS One* **10**, e0127360 (2015).
521 32. Bourin M, Chue P, Guillon Y. Paroxetine: a review. *CNS Drug Rev* **7**, 25-47
522 (2001).
523 33. Coleman JA, Green EM, Gouaux E. X-ray structures and mechanism of the
524 human serotonin transporter. *Nature* **532**, 334-339 (2016).
525 34. Coleman JA, Navratna V, Antermite D, Yang D, Bull JA, Gouaux E. Chemical
526 and structural investigation of the paroxetine-human serotonin transporter
527 complex. *Elife* **9**, e56427 (2020).
528 35. Lillesaar C, Stigloher C, Tannhauser B, Wullimann MF, Bally-Cuif L. Axonal
529 projections originating from raphe serotonergic neurons in the developing and
530 adult zebrafish, Danio rerio, using transgenics to visualize raphe-specific pet1
531 expression. *J Comp Neurol* **512**, 158-182 (2009).
532 36. Obholzer N*, et al.* Vesicular glutamate transporter 3 is required for synaptic
533 transmission in zebrafish hair cells. *J Neurosci* **28**, 2110-2118 (2008).
534 37. Sato T, Takahoko M, Okamoto H. HuC:Kaede, a useful tool to label neural
535 morphologies in networks in vivo. *Genesis* **44**, 136-142 (2006).
536 38. Mercurio S, Serra L, Pagin M, Nicolis SK. Deconstructing Sox2 Function in
537 Brain Development and Disease. *Cells* **11**, 1604 (2022).
538 39. Zhu S, Korzh V, Gong Z, Low BC. RhoA prevents apoptosis during zebrafish
539 embryogenesis through activation of Mek/Erk pathway. *Oncogene* **27**, 1580-
540 1589 (2008).
541 40. Escamilla CO*, et al.* Kctd13 deletion reduces synaptic transmission via
542 increased RhoA. *Nature* **551**, 227-231 (2017).
543 41. Amar M*, et al.* Autism-linked Cullin3 germline haploinsufficiency impacts
544 cytoskeletal dynamics and cortical neurogenesis through RhoA signaling. *Mol*
545 *Psychiatry* **26**, 3586-3613 (2021).
546 42. Scott EK*, et al.* Targeting neural circuitry in zebrafish using GAL4 enhancer
547 trapping. *Nat Methods* **4**, 323-326 (2007).
548 43. Sato T, Hamaoka T, Aizawa H, Hosoya T, Okamoto H. Genetic single-cell
549 mosaic analysis implicates ephrinB2 reverse signaling in projections from the
550 posterior tectum to the hindbrain in zebrafish. *J Neurosci* **27**, 5271-5279 (2007).

551 44. Niell CM, Meyer MP, Smith SJ. In vivo imaging of synapse formation on a
552 growing dendritic arbor. *Nat Neurosci* **7**, 254-260 (2004).
553 45. Hua JY, Smear MC, Baier H, Smith SJ. Regulation of axon growth in vivo by
554 activity-based competition. *Nature* **434**, 1022-1026 (2005).
555 46. Avino TA*, et al.* Neuron numbers increase in the human amygdala from birth to
556 adulthood, but not in autism. *Proc Natl Acad Sci U S A* **115**, 3710-3715 (2018).
557 47. Lal P*, et al.* Identification of a neuronal population in the telencephalon essential
558 for fear conditioning in zebrafish. *BMC Biol* **16**, 45 (2018).
559 48. Suh H, Consiglio A, Ray J, Sawai T, D'Amour KA, Gage FH. In vivo fate
560 analysis reveals the multipotent and self-renewal capacities of Sox2+ neural
561 stem cells in the adult hippocampus. *Cell Stem Cell* **1**, 515-528 (2007).
562 49. Sahay A, Hen R. Adult hippocampal neurogenesis in depression. *Nat Neurosci*
563 **10**, 1110-1115 (2007).
564 50. Boldrini M*, et al.* Hippocampal angiogenesis and progenitor cell proliferation
565 are increased with antidepressant use in major depression. *Biol Psychiatry* **72**,
566 562-571 (2012).
567 51. Persico AM*, et al.* Reduced programmed cell death in brains of serotonin
568 transporter knockout mice. *Neuroreport* **14**, 341-344 (2003).
569 52. Levkovitz Y, Gil-Ad I, Zeldich E, Dayag M, Weizman A. Differential induction
570 of apoptosis by antidepressants in glioma and neuroblastoma cell lines: evidence
571 for p-c-Jun, cytochrome c, and caspase-3 involvement. *J Mol Neurosci* **27**, 29-42
572 (2005).
573 53. Schuster C*, et al.* Selective serotonin reuptake inhibitors--a new modality for the
574 treatment of lymphoma/leukaemia? *Biochem Pharmacol* **74**, 1424-1435 (2007).
575 54. Wei P*, et al.* Fluvoxamine prompts the antitumor immune effect via inhibiting
576 the PD-L1 expression on mice-burdened colon tumor. *Cell Biol Int* **47**, 439-450
577 (2023).
578 55. Hodge JM*, et al.* Selective serotonin reuptake inhibitors inhibit human osteoclast
579 and osteoblast formation and function. *Biol Psychiatry* **74**, 32-39 (2013).
580 56. Reis G*, et al.* Effect of early treatment with fluvoxamine on risk of emergency
581 care and hospitalisation among patients with COVID-19: the TOGETHER
582 randomised, platform clinical trial. *Lancet Glob Health* **10**, e42-e51 (2022).
583 57. Hashimoto Y, Suzuki T, Hashimoto K. Mechanisms of action of fluvoxamine for
584 COVID-19: a historical review. *Mol Psychiatry* **27**, 1898-1907 (2022).
585 58. Sato T, Ito T, Handa H. Cereblon-Based Small-Molecule Compounds to Control
586 Neural Stem Cell Proliferation in Regenerative Medicine. *Front Cell Dev Biol* **9**,

587 629326 (2021).
588 59. Ito T, Yamaguchi Y, Handa H. Exploiting ubiquitin ligase cereblon as a target for
589 small-molecule compounds in medicine and chemical biology. *Cell Chem Biol*
590 **28**, 987-999 (2021).
591 60. Salichon N*, et al.* Excessive activation of serotonin (5-HT) 1B receptors disrupts
592 the formation of sensory maps in monoamine oxidase a and 5-ht transporter
593 knock-out mice. *J Neurosci* **21**, 884-896 (2001).
594 61. Upton AL*, et al.* Lack of 5-HT(1B) receptor and of serotonin transporter have
595 different effects on the segregation of retinal axons in the lateral geniculate
596 nucleus compared to the superior colliculus. *Neuroscience* **111**, 597-610 (2002).
597 62. Aizawa H, Goto M, Sato T, Okamoto H. Temporally regulated asymmetric
598 neurogenesis causes left-right difference in the zebrafish habenular structures.
599 *Dev Cell* **12**, 87-98 (2007).
600 63. Xiao T, Baier H. Lamina-specific axonal projections in the zebrafish tectum
601 require the type IV collagen Dragnet. *Nat Neurosci* **10**, 1529-1537 (2007).
602 64. Ito T*, et al.* Identification of a primary target of thalidomide teratogenicity.
603 *Science* **327**, 1345-1350 (2010).
604 65. Dreosti E, Lopes G, Kampff AR, Wilson SW. Development of social behavior in
605 young zebrafish. *Front Neural Circuits* **9**, 39 (2015).
606 66. Kriegstein A, Alvarez-Buylla A. The glial nature of embryonic and adult neural
607 stem cells. *Annu Rev Neurosci* **32**, 149-184 (2009).
608 67. Asatsuma-Okumura T*, et al.* p63 is a cereblon substrate involved in thalidomide
609 teratogenicity. *Nat Chem Biol* **15**, 1077-1084 (2019).
610 68. Miller MT, Strömland K, Ventura L, Johansson M, Bandim JM, Gillberg C.
611 Autism with ophthalmologic malformations: the plot thickens. *Trans Am*
612 *Ophthalmol Soc* **102**, 107-120; discussion 120-101 (2004).
613
614
615

Acknowledgements

We are grateful to Hiroshi Handa, Keisuke Miyazawa, Masaki Hiramoto (Tokyo Medical University) for valuable discussions and generous support. We thank members of Anatomy and Experimental Animals (Saitama Medical University) and Hiromi Kazama (Tokyo Medical University) for help and technical support. Tg(*elavl3:Kaede*), Tg(*pou4fl-hsp70l:GFP*), Tg*(gfap:Gal4FF;UAS:GFP*) and SAGFF120A were provided from Zebrafish National BioResource Project. Tg(*pou4f3:GAL4;UAS:mCherry*) were provided by Herwig Baier. This work was supported by JSPS KAKENHI Grant Numbers 18K09271 (to T.S. and T.Ka.), 22K09625 (to T.S., S.T., T.Ku. and T. Ka.), Saitama Medical University support grant for collaboration with Saitama University 21-J-04 (to T.S. and S.T.), 23-J-03 (to T.S., S.T. and T.Ka.), and Research Grant from Saitama Medical University 27-B-1-29 (to T.S.).

Author contributions

T.S. conceived and designed the experiments. T.S., T.Ku. performed the anatomy and pharmacology experiments, and K.S., T.O. performed behavioral experiments. T.S., K.S., S.T. analyzed the data. T.S., S.T., T.Ka., and M.N. wrote and edited the manuscript.

Competing interests

The authors declare no competing interests.

645 **Figure Legends**

646

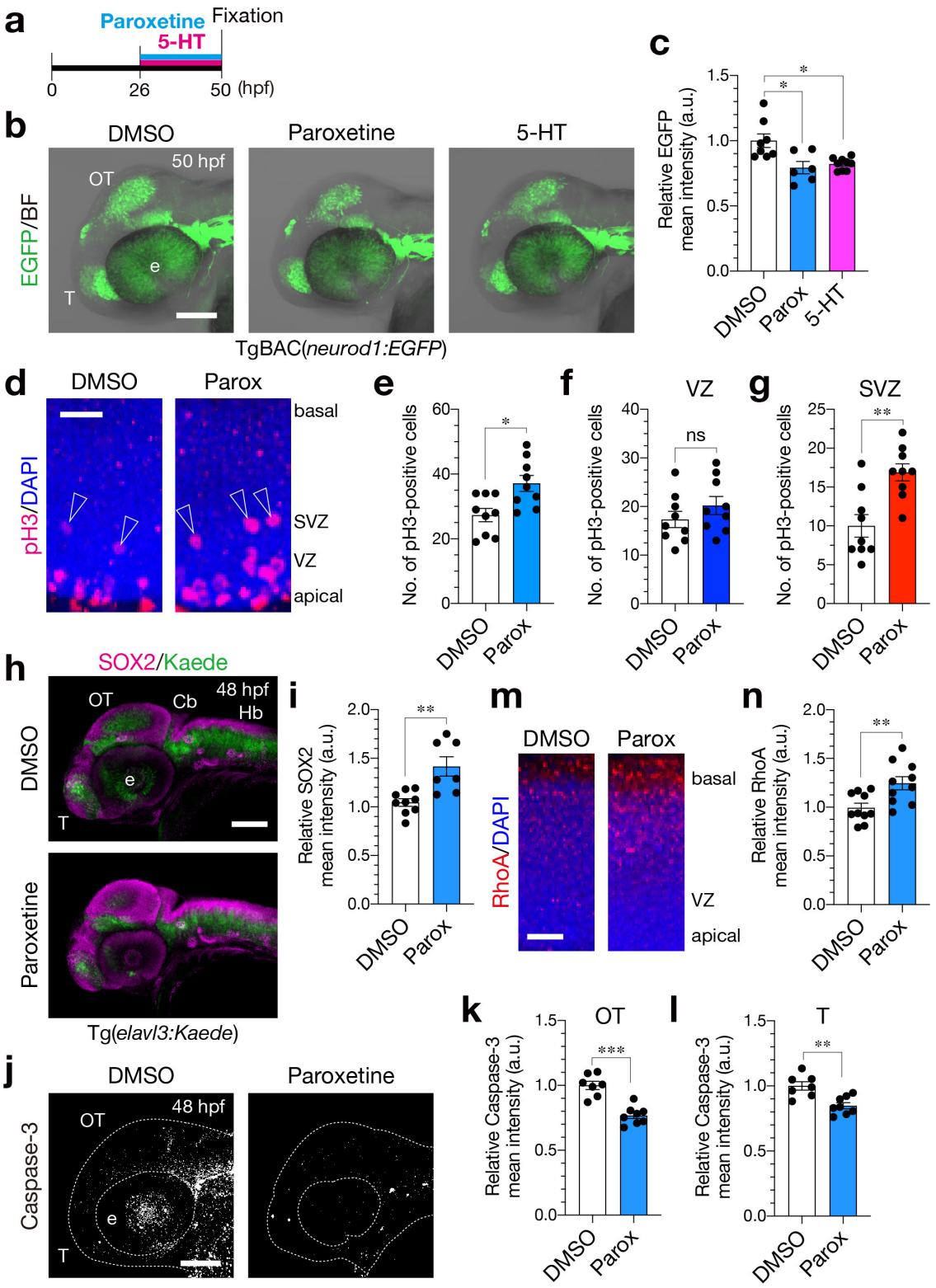

647

648 **Figure 1.** Paroxetine suppresses neurogenesis and apoptosis to promote the proliferation

of neural progenitor cells in the optic tecta of zebrafish embryos. **a** A schematic diagram of the treatment of zebrafish early-stage embryos with parox or 5-HT. **b** Lateral views of 50-hpf TgBAC(*neurod1:EGFP*) embryos treated with parox, 5-HT, or DMSO (the control). **c** Quantification of the mean EGFP intensity in the optic tecta of the transgenic embryos. Kruskal-Wallis with Dunn's multiple comparisons tests. **d** High-magnification images of the optic tecta of zebrafish embryos treated with DMSO or parox and immunostained for pH3 (red), with DAPI (blue) co-staining for the nuclei. Open arrowheads, pH3-positive cells in the SVZ. **e**–**g** Quantification of the number of pH3-positive cells in the optic tecta (**e**), the ventricular zones (**f**), and the subventricular zones (**g**). **h** Lateral views of DMSO- or parox-treated embryos immunostained for SOX2 (red). **i** Quantification of the mean intensities of SOX2 signals in the zebrafish brains. **j** Lateral views of DMSO- or parox-treated embryos immunostained for active Caspase-3 (white puncta) at 48 hpf. Images binarized above a threshold. Dotted line: Morphological outlines. **k**, **l** Quantification of the mean intensities of active Caspase-3 in the optic tecta (**k**) and telencephalons (**l**) of the treated embryos. **m** High-magnification images of the optic tecta immunostained for RhoA (red) and co-stained with DAPI (blue). **n** Quantification of the mean intensities of the RhoA signals in the optic tecta. Scale bars: 100 μm (**b**, **h**, **j**); 25 μm (**d, m**). Data are presented as mean ± SEM. $*p < 0.05$, $**p < 0.01$, $***p < 0.001$; ns, not significant. Mann-Whitney U test; 5-HT, serotonin; Cb, cerebellum; DAPI, 4′,6-diamidino-2-phenylindole fluorescent stain; DMSO, dimethylsulfoxide; e, eye; EGFP, enhanced green fluorescent protein; Hb, hindbrain; hpf, hours post-fertilization; OT, optic tectum; parox, paroxetine; pH3, phospho-histone H3; SEM, standard error of the mean; SVZ, subventricular zone; T, telencephalon; VZ, ventricular zone.

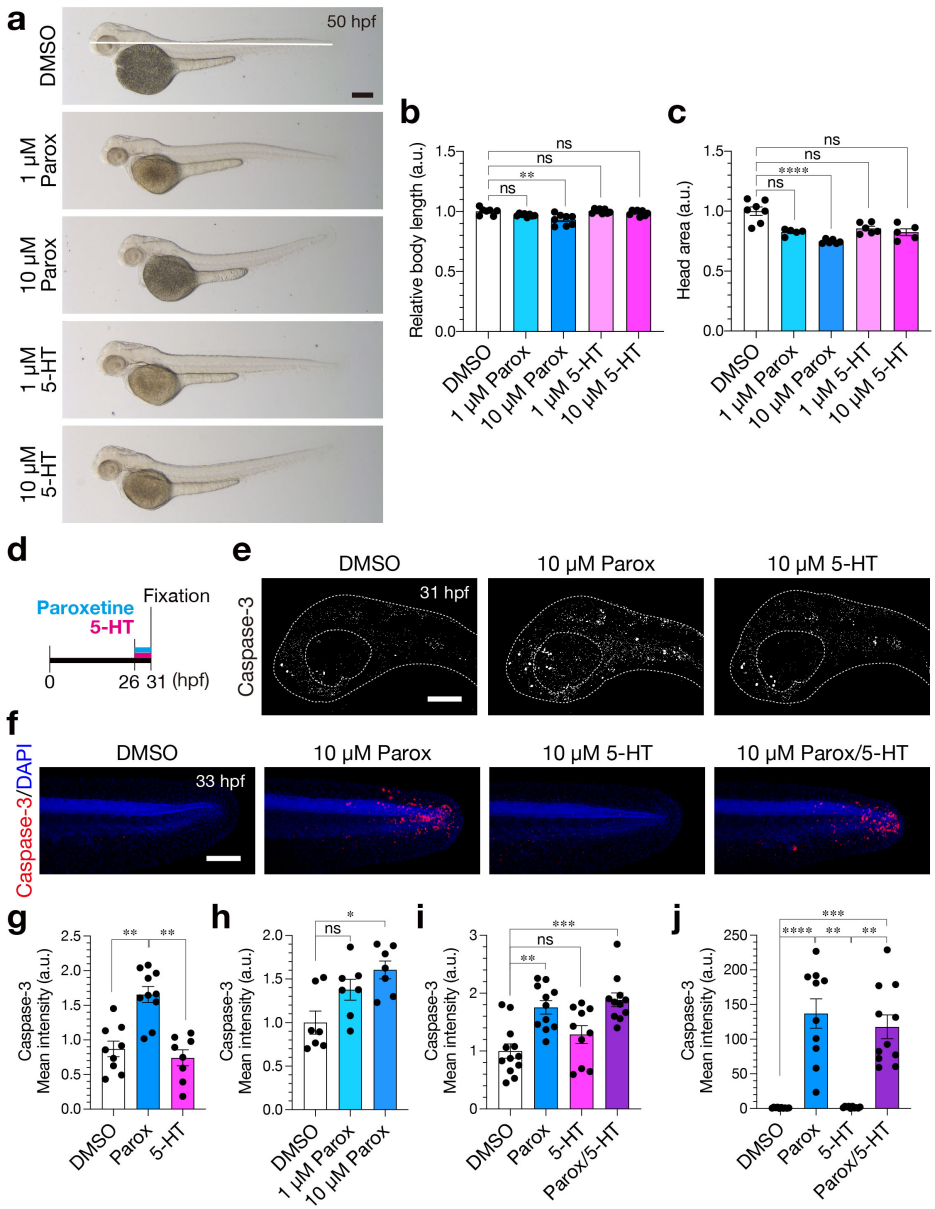

Figure 2. Paroxetine restricts embryonic growth by inducing local apoptosis in the brain and tail tip of zebrafish embryos. **a** Lateral views of 50-hpf zebrafish embryos treated with parox, 5-HT, or DMSO (control). **b, c** Quantification of the body lengths (**b**) and head areas (**c**) of the treated embryos. **d** A scheme for the experiment. **e** Lateral views of the heads of 31-hpf embryos treated with DMSO, parox, or 5-HT and immunostained for active Caspase-3 (white puncta). Images binarized above a threshold. Dotted line: Morphological outlines. **f** Lateral views of the tail tips of 33-hpf embryos treated with DMSO, parox, or 5-HT and immunostained for active Caspase-3. Anterior, left; posterior, right. **g–j** Quantification of the mean intensities of active Caspase-3 signals in the heads (**g–i**) and tail tips (**j**). Scale bars: 200 μm (**a**); 100 μm (**e**, **f**). Data are presented as mean

685 ± SEM. *$p < 0.05$, **$p < 0.01$, ****$p < 0.0001$; ns, not significant. Kruskal-Wallis with
686 Dunn's multiple comparisons tests; 5-HT, serotonin; DMSO, dimethylsulfoxide; hpf,
687 hours post-fertilization; parox, paroxetine; SEM, standard error of the mean.
688

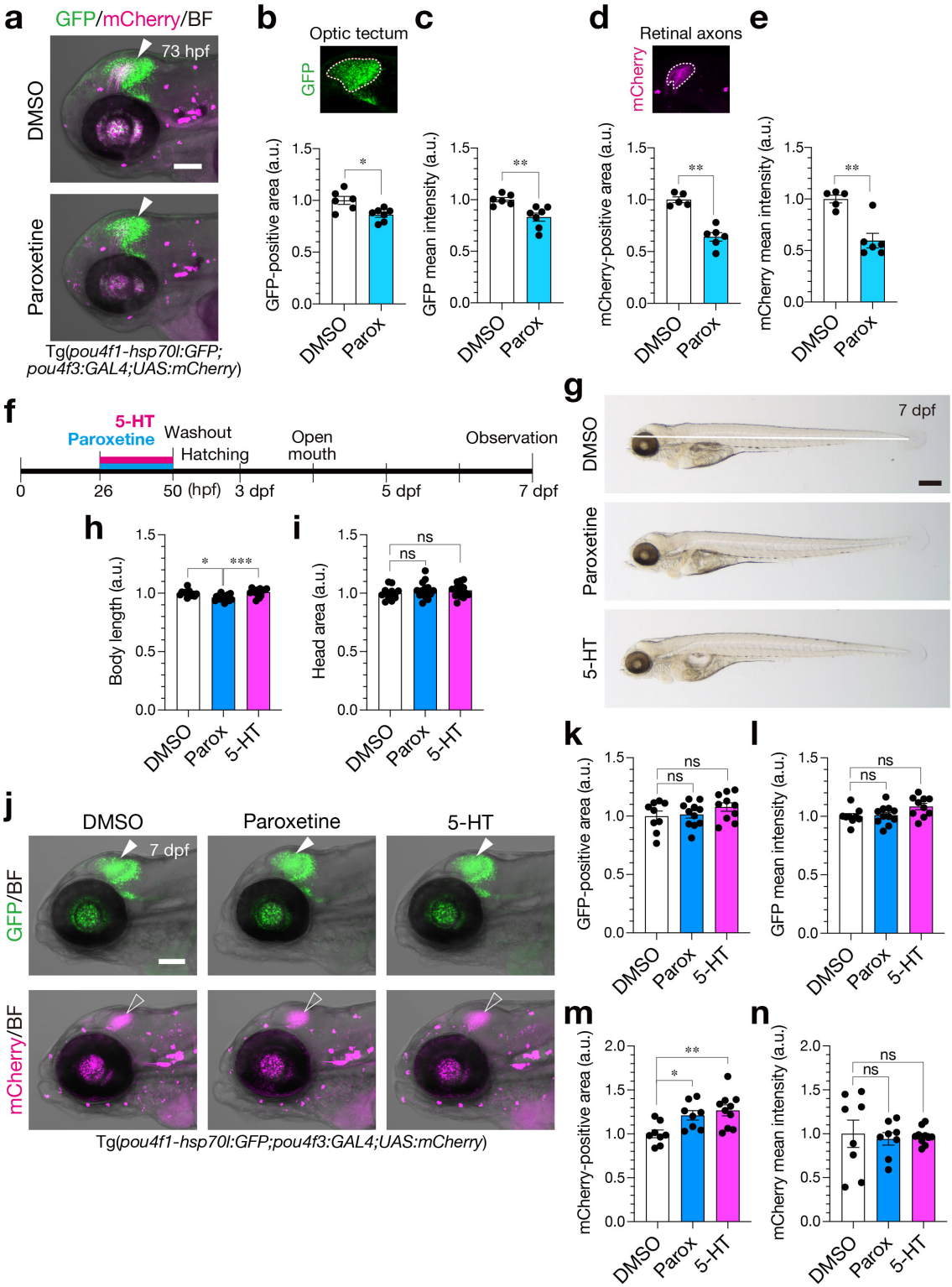

Figure 3. Early transient paroxetine inhibiting the development of the retinotectal projection leads to brain-preferential remodeling. **a** Lateral views of the heads of 73-hpf Tg(*pou4fl-hsp70l:GFP; pou4f3:GAL4;UAS:mCherry*) embryos treated with DMSO or parox at 1 μM for 2 days from 26 hpf. Tectal neurons and retinal axons express GFP

694 (green) and retinal axons express mCherry (magenta). **b** Quantification of the GFP-
695 positive areas. **c** Mean GFP intensities in the optic tecta of the transgenic embryos. **d**
696 Quantification of the mCherry-positive areas. **e** Mean mCherry intensities in the optic
697 tecta of the transgenic embryos. **b, d** Top: A representative image of the quantified area
698 (dotted circle) in the optic tectum. Mann-Whitney U test. **f** Scheme for the treatment
699 schedule and major developmental events in the zebrafish. **g** Lateral views of 7-dpf larvae
700 treated with parox, 5-HT, or DMSO. **h**, **i** Quantification of the body lengths (**h**) and head
701 areas (**i**) of the treated embryos. **j** Lateral views of the heads of 7-dpf Tg(*pou4f1-*
702 *hsp70l:GFP; pou4f3:GAL4;UAS:mCherry*) larvae treated with parox, 5-HT, or DMSO
703 (control). Optic tecta (filled arrowheads) and retinal axons (open arrowheads). **k**–**n**
704 Quantification of the GFP-positive areas (**k**), the mean GFP intensities (**l**), the mCherry-
705 positive areas (**m**), and the mean mCherry intensities (**n**) in the optic tecta of the
706 transgenic larvae. Kruskal-Wallis with Dunn's multiple comparisons tests; Scale bar, 100
707 μm. Data are presented as mean ± SEM. *$p < 0.05$, **$p < 0.01$; ns, not significant. 5-HT,
708 serotonin; DMSO, dimethylsulfoxide; GFP, green fluorescent protein; hpf, hours post-
709 fertilization; parox, paroxetine; SEM, standard error of the mean.
710

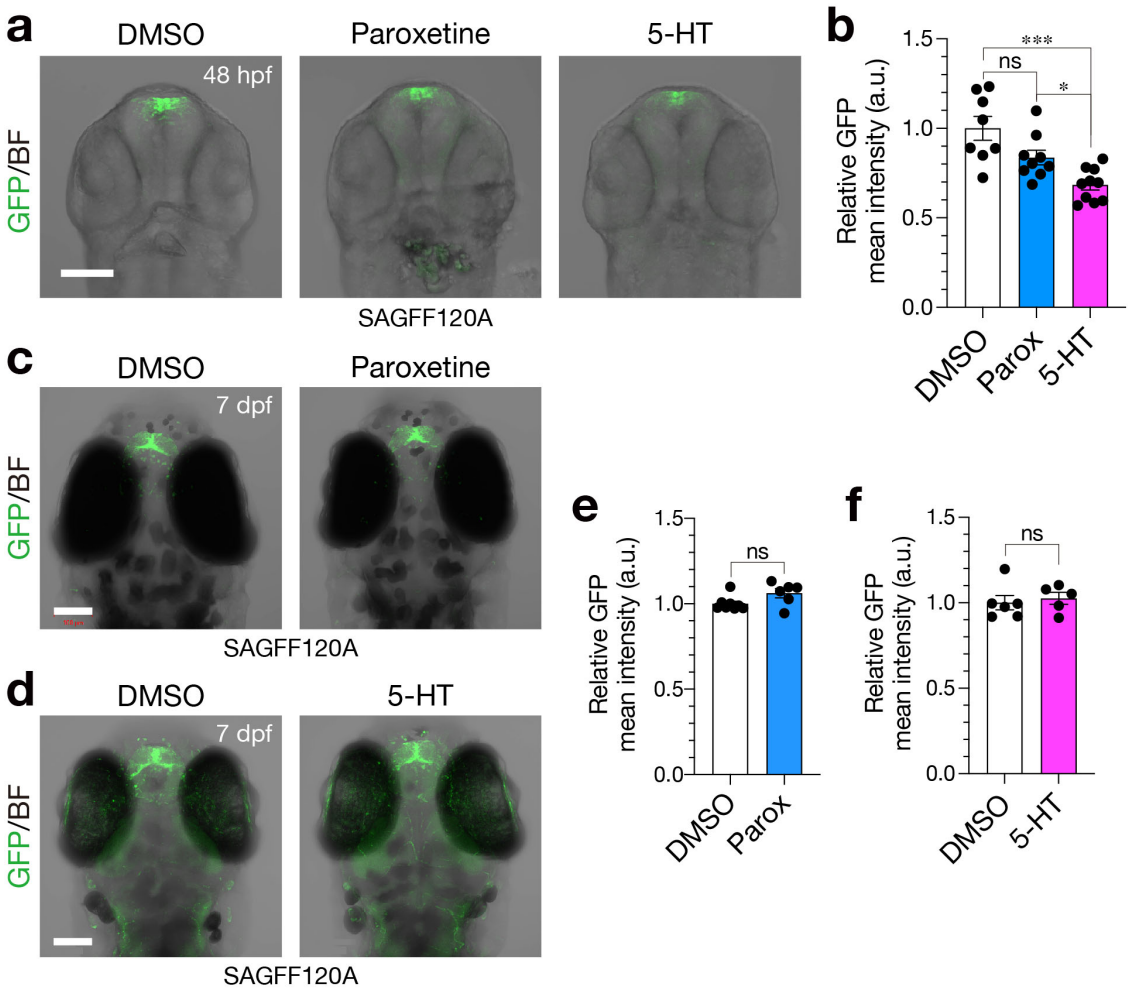

Figure 4. Paroxetine exerts its effects on the dorsal telencephalon in a manner similar to the optic tectum. **a** Dorsal views of 48-hpf SAGFF120A;UAS:GFP zebrafish embryos treated with parox, 5-HT, or DMSO (control). **b** Quantification of the mean GFP intensities in the dorsal telencephalons of SAGFF120A;UAS:GFP zebrafish embryos. Kruskal-Wallis with Dunn's multiple comparisons tests. **c** Dorsal views of 7-dpf SAGFF120A;UAS:GFP larvae treated with paroxetine. **d** Dorsal views of 7-dpf SAGFF120A;UAS:GFP larvae treated with 5-HT. **e** Quantification of the mean GFP intensities in the dorsal telencephalons. $p = 0.1419$, Mann-Whitney U test. **f** Quantification of the mean GFP intensities in the dorsal telencephalons. $p = 0.6623$, Mann-Whitney U test. Scale bar, 100 µm. Data are presented as mean ± SEM. *$p < 0.05$, ***$p < 0.001$; ns, not significant. 5-HT, serotonin; DMSO, dimethylsulfoxide; GFP, green fluorescent protein; hpf, hours post-fertilization; parox, paroxetine; SEM, standard error of the mean.

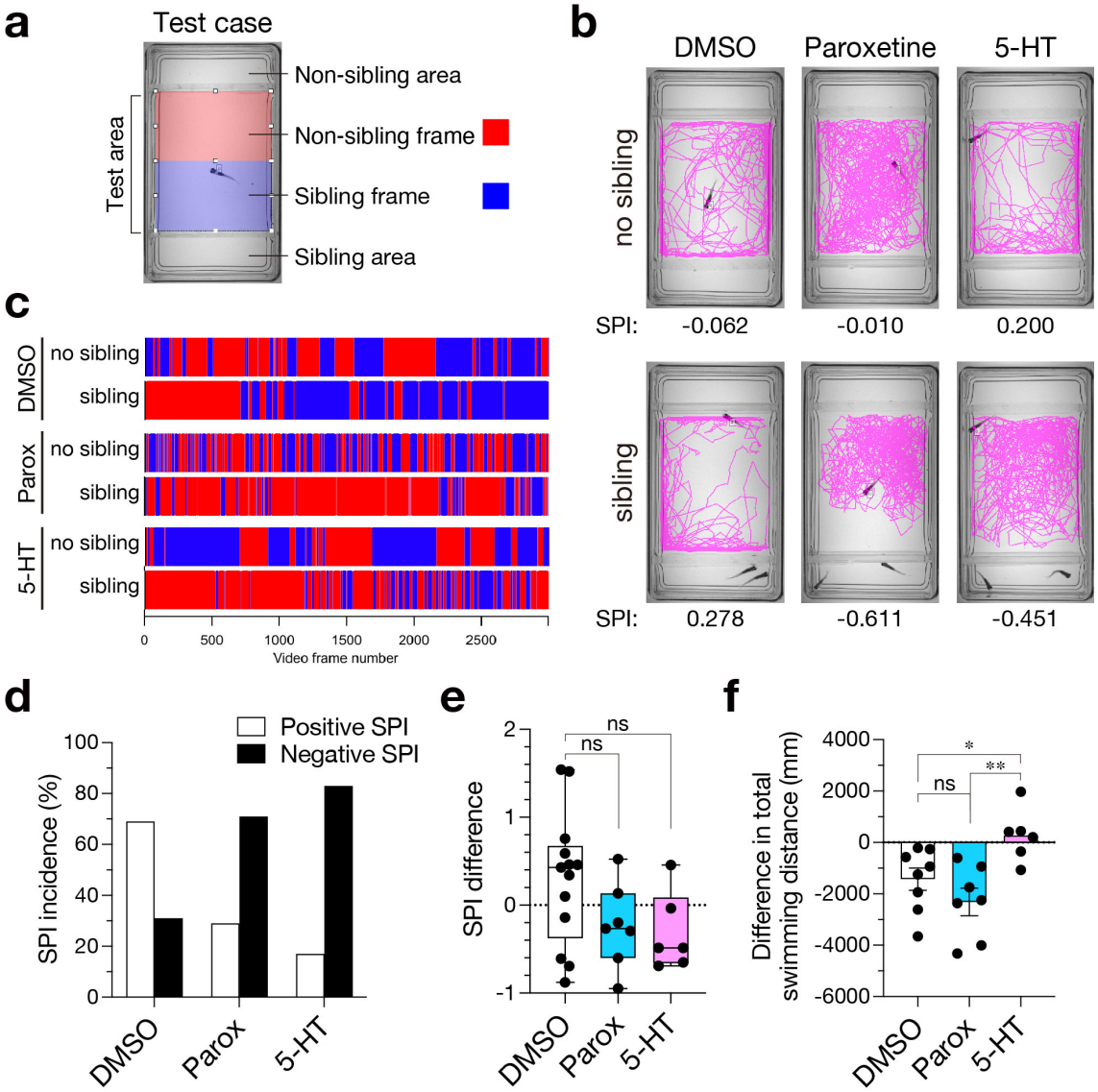

Figure 5. Early transient paroxetine- and 5-HT-treated zebrafish exhibit a tendency to impaired social behavior**. a** A test case used in this study. The sibling frame shown in blue, the non-sibling frame shown in red. **b** Representative swimming trajectories of the fish treated with DMSO (control), parox, or 5-HT in the non-sibling (top) and sibling trials (bottom). The SPIs indicated below. **c** A total of 2,998 frames recorded over 5 min for the trials shown in (**b**) with color-coded according to the frames in (**a**). **d** The incidences of positive SPI (sibling > non-sibling, white) and negative SPI (sibling < non-sibling, black) in the fish treated with DMSO, parox, and 5-HT (n = 13, 7, 6, respectively). **e** Differences in SPIs between the sibling and non-sibling trials. Data are presented as mean ± SEM, $p = 0.0456$, Brown-Forsythe ANOVA test. **f** Differences in the total swimming trajectory distances of the fish between the sibling and non-sibling trials. Data are presented as mean ± SEM, $*p < 0.05$, $**p < 0.01$; ns, not significant. Brown-Forsythe with Dunnett's

739 multiple comparisons tests. 5-HT, serotonin; ANOVA, analysis of variance; DMSO,
740 dimethylsulfoxide; GFP, green fluorescent protein; hpf, hours post-fertilization; parox,
741 paroxetine; SEM, standard error of the mean; SPI, social preference index.
742
743
744